Dalton Transactions

ROYAL SOCIETY OF CHEMISTRY

PAPER

View Article Online
View Journal | View Issue

Cite this: *Dalton Trans.*, 2025, **54**, 5025

Redox-active tin(II) complexes with sterically demanding *o*-phenylenediamido ligands and their reactivity with organic azides†

Hideki Sugimoto, *[a] Akira Yoneda, [a] Mayuka Yano,[a] Kazunobu Sato, *[b] Yoshihito Shiota, [c] Mayuko Miyanishi,[c] Kazunari Yoshizawa *[c] and Shinobu Itoh *[a]

A series of tin(II) complexes ^{R}**1** supported by phenylene-1,2-diamido ligands containing a bulky *N*-substituent TIPT (2,4,2′′,4′′-tetraisopropyl-[1,1′:3′,1′′]terphenyl) and different aromatic substituents R (Cl, H, Me, OMe) at the 4,5-positions and by a naphthalene-2,3-diamido ligand with the TIPT substituent ^{naph}**1** are synthesised and characterised. Tin(II) complexes **SnL^{Me}** and **SnL$^{Ph(tBu)2}$** supported by phenylene-1,2-diamido ligands with sterically less hindered *N*-substituents, Ph or 3,5-di-*tert*-butylphenyl, are also prepared as reference complexes. Crystal structures of ^{R}**1** and ^{naph}**1** show that the tin(II) centers are coordinated with the two amido nitrogen atoms of the respective deprotonated chelating ligand and two solvent molecules such as tetrahydrofuran and/or acetonitrile. On the other hand, the tin(II) complex **SnL$^{Ph(tBu)2}$** contains only one coordinating solvent molecule, and its tin(II) center exhibits intermolecular interaction with the aromatic ligand moiety of a neighboring tin(II) complex through a 5p–π interaction. The ^{119}Sn NMR signal of ^{R}**1** in C_6D_6 shifts from the lower- to higher-magnetic field region as R becomes more electron-withdrawing, which can be explained by assuming that the naked two-coordinate tin(II) complex and solvent-involving three- and/or four-coordinate tin(II) complex exist in equilibrium in solution. The tin(II) complexes with the sterically demanding ligands (^{R}**1** and ^{naph}**1**) are more stabilised against hydrolysis when compared with **SnL^{Ph}** and **SnL$^{Ph(tBu)2}$**. The tin(II) complexes ^{R}**1** and ^{naph}**1** undergo one-electron quasi-reversible ligand-based redox oxidation in a range from −0.45 V to +0.13 V *vs.* Fc/Fc^{+}. The tin(II) complexes having electron-donating groups (R = OMe, Me, H) exhibit intramolecular C–H amination reactivity when treated with trisylazide (2,4,6-triisopropylphenylsulfonyl azide), giving sultam (5,7-diisopropyl-2,3-dihydro-3,3-dimethyl-1,2-benzothiazole-1,1-dioxide) as the product. On the other hand, the tin(II) complexes having electron-withdrawing groups (R = Cl, naph) do not show such reactivity. Such a difference in the reactivity is attributed to availability of a nitrene-radical bound species formed by the reaction. The formation step of the nitrene-radical bound species is analyzed kinetically to reveal that the reaction comprises two steps: binding of the organic azide to the tin(II) centre and successive intramolecular electron transfer from the ligand to the azide moiety to induce dinitrogen (N_2) elimination and nitrene-radical formation.

Received 14th January 2025,
Accepted 7th February 2025

DOI: 10.1039/d5dt00100e

rsc.li/dalton

Introduction

Metal complexes with redox-active ligands have attracted much recent attention in current synthetic organic chemistry as well as coordination chemistry, since such ligands can avoid high activation barriers in several types of redox transformation reactions.[1–4] Tyrosine in the oxygen-evolving center of photosystem II and galactose oxidase,[5,6] porphyrin in cytochrome P450,[7] and dithiolene in molybdoenzymes[8] are typical examples of such redox-active ligands in nature. In coordination chemistry, redox-active ligands have been recognized as being able to offer nobility to base metals by combining a 1e^{-}

[a]*Department of Molecular Chemistry, Division of Applied Chemistry, Graduate School of Engineering, Osaka University, Yamadaoka, Suita, Osaka 565-0871, Japan. E-mail: sugimoto@chem.eng.osaka-u.ac.jp, shinobu@chem.eng.osaka-u.ac.jp*
[b]*Department of Chemistry, Graduate School of Science, Osaka Metropolitan University, 3-3-138, Sugimoto, Sumiyoshi-ku, Osaka 558-8585, Japan. E-mail: sato@omu.ac.jp*
[c]*Institute for Materials Chemistry and Engineering and International Research Center for Molecular System, Kyushu University, Motooka, Nishi-ku, Fukuoka, 819-0395, Japan. E-mail: kazunari@ms.ifoc.kyushu-u.ac.jp*

†Electronic supplementary information (ESI) available: Tables S1–S9, Fig. S1–S11. Cartesian coordinates. CCDC 2325047–2325051. For ESI and crystallographic data in CIF or other electronic format see DOI: **https://doi.org/10.1039/d5dt00100e**

redox change at both the ligand and the metal center for an overall $2e^-$ redox process.[1–4,9] This methodology has been applied to alkane and arene amination and alkene aziridination reactions, where metal-nitrenoids are involved as the active oxidant.[1,3,10] On the other hand, recent studies on reactions of dπ-filled late-transition metal complexes with redox-active ligands containing an organic azide have demonstrated that only the $1e^-$ redox change occurs at the redox-active ligand without a change of the metal oxidation state to enable formation of metal-nitrenoids.[11–20] In these reactions, the one-electron transfer takes place from the redox-active ligand to the bound organic azide to induce dinitrogen (N_2) elimination. The metal-nitrenoids generated by these reactions feature a radical-localizing nitrene unit, namely a nitrene-radical bound metal complex, and this has attracted current interest in view of its unique electronic structure as well as its radical type of reactivity. Such nitrene-radical bound metal complexes were proposed as reactive intermediates, based on DFT calculation studies, in C(sp^3)–H amination with organic azides catalyzed by the dπ-filled palladium(II) and rhodium(III) complexes coordinated with redox-active ligands (Fig. 1(a) and (b)).[11–14] Recently, a nitrene-radical bound cobalt(III) complex of a redox-active tetra-amido macrocyclic ligand, which was active in aziridination and sulfimidation, was characterised spectroscopically (Fig. 1(c)).[17–19] These results suggest that this methodology can be applied to complexes of redox-innocent main group elements. The tin(II) ion has a $(5s)^2$ lone pair highly stabilized by the relativistic effect and is essentially inactive against an electron transfer type of oxidation although some exceptions have been reported.[21,22] In this context, we have recently reported that the reaction of a tin(II) complex of a sterically demanding phenylene-1,2-diamido-based ligand with an organic azide enables formation of a nitrene-radical bound tin(II) complex (Fig. 1(d)), which exhibited C–H activation reactivity.[23] As in the case of the nitrene-radical bound palladium(II), rhodium(III), and cobalt(III) complexes,[11,13,17] formation of the nitrene-radical bound tin(II) complex is induced by electron transfer from the redox-active ligand.[23]

Whereas tin(II) complexes comprising phenylene-1,2-diamido ligands have been reported,[24–30] research interest is limited to their nature as Lewis bases using the $(5s)^2$ lone pair or Lewis acids using the empty ($5p_z$) orbital,[31] but little attention has been directed toward functions of the redox non-innocent phenylene-1,2-diamido ligands. In this study, we synthesise and characterise a series of tin(II) complexes ^{R}**1** supported by phenylene-1,2-diamido ligands containing a sterically demanding *N*-substituent TIPT (2,4,2″,4″-tetraisopropyl-[1,1′:3′,1″]terphenyl) and different aromatic substituents R (Cl, H, Me, OMe) at the 4,5-positions as well as the tin(II) complex of a naphthalene-2,3-diamido ligand with TIPT ^{naph}**1** (Fig. 2). The TIPT substituent has been shown to provide a hydrophobic space around a first coordination sphere of the metal centre and prevent intermolecular interaction of the metal centre to stabilize the mononuclear structure.[23,32–34] The tin(II) complexes of phenylene-1,2-diamido ligands containing less bulky *N*-substituents, **SnL**^{Ph} and **SnL**$^{Ph(tBu)2}$, are also prepared as reference complexes. Examination of their electrochemical properties as well as their reactivities with organic azides gives further insights into the roles of redox-active ligands in the reactions of main group element complexes.

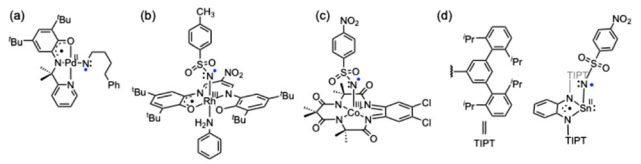

Fig. 1 (a)–(d) Reported nitrene-radical complexes coordinated with redox-active ligands.

Results and discussion

Preparation, characterization, and crystal structures of tin(II) complexes

Tin(II) complexes ^{Cl}**1**, ^{Me}**1**, ^{OMe}**1**, ^{naph}**1** and **SnL**$^{Ph(tBu)2}$ were synthesised by a ligand exchange reaction between $Sn[N(SiMe_3)_2]_2$ and $^{R}LH_2$ (R = Cl, Me, OMe and naph) or $L^{Ph(tBu)2}H_2$. The obtained complexes were characterised by ^{1}H, ^{13}C, and ^{119}Sn NMR spectroscopy as well as elemental analysis. In the ^{1}H NMR spectra of all the complexes in C_6D_6, ^{1}H signals of all C–H protons of the ligands appeared but the N–H proton signals of $^{R}LH_2$ disappeared, indicating that isolated tin(II) complexes have the deprotonated diamido ligand, $(^{R}L)^{2-}$ or $(L^{Ph(tBu)2})^{2-}$, as in the case of ^{H}**1** (see Experimental section and Fig. S1–S4†).[23] Single crystals of the tin(II) complexes were obtained by slow diffusion of acetonitrile into a THF solution of each complex. The ORTEP drawings of the X-ray crystal structures are depicted in Fig. 3. The crystal structures of ^{Cl}**1**, ^{Me}**1**, ^{OMe}**1** and ^{naph}**1** reveal that overall they all resemble that of ^{H}**1** exhibiting a stannylene-type structure with the two coordinating nitrogen atoms of the diamido unit as previously reported (Fig. 3(a)–(d)). But there are some structural differences when compared with the structures of the related stannylene com-

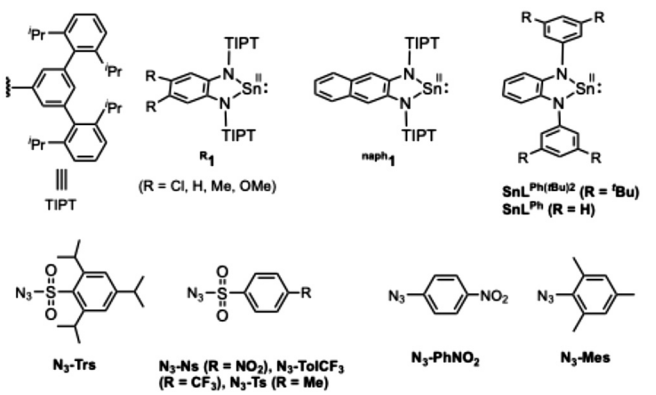

Fig. 2 ChemDraw structures of the tin(II) complexes and organic azides employed in this study and their abbreviations.

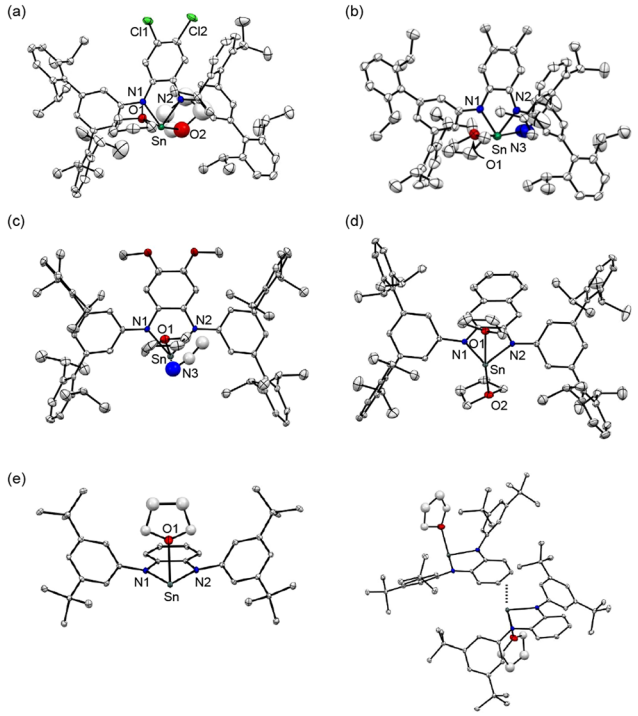

Fig. 3 ORTEP diagrams of (a) [Sn(^{Cl}L)(THF)$_2$] (^{Cl}**1**), (b) [Sn(^{Me}L)(THF)(CH$_3$CN)] (^{Me}**1**), (c) [Sn(^{OMe}L)(THF)(CH$_3$CN)] (^{OMe}**1**), (d) [Sn(^{naph}L)(THF)$_2$] (^{naph}**1**) and (e) [Sn(L$^{Ph(tBu)2}$)(THF)] (**SnL$^{Ph(tBu)2}$**) showing 50% ellipsoids. Hydrogen atoms and non-coordinating solvent molecules are omitted for clarity.

plexes coordinated with the less hindered *o*-phenylenediamido ligands reported in the literature.[24–30] Namely, due to the sterically demanding TIPT substituents, there is no intermolecular interaction in the ^{R}L ligand system to allow coordination of two solvent molecules with each tin(II) centre. In ^{Cl}**1** and ^{naph}**1**, the two apical positions are occupied with two THF molecules. With respect to ^{Me}**1** and ^{OMe}**1**, one coordinating solvent molecule is THF while the other one is CH$_3$CN. In the case of **SnL$^{Ph(tBu)2}$**, on the other hand, one of the apical positions is ligated with one THF molecule but the opposite apical site is occupied by the phenylenediamido ring of a neighboring tin (II) complex (Fig. 3(e)). The closest distance between the tin(II) centre and the aromatic ring of the neighboring complex is 2.85 Å, confirming an intermolecular interaction between the empty 5p$_z$-orbital of tin(II) and a π-orbital of the phenylenediamido unit. Apparently, the sterically demanding TIPT substituent prohibits such an intermolecular interaction to stabilize the monomer structure of ^{R}**1** as mentioned in the Introduction.

The ^{119}Sn NMR spectra of C$_6$D$_6$ solutions of ^{Cl}**1**, ^{H}**1**, ^{Me}**1**, ^{OMe}**1** and ^{naph}**1** were recorded to evaluate the coordination environments of the tin(II) centers (Fig. S5†). The ^{119}Sn signals appeared at 26 ppm, 65 ppm, 83 ppm, 126 ppm and 54 ppm, respectively, which are listed in Table 1 together with those of the related stannylene complexes.[24–30] It has been reported that a ^{119}Sn chemical shift of stannylene is largely related to

Table 1 ^{119}Sn chemical shifts of the tin(II) complexes and related compounds

Complex	^{119}Sn shift/ppm
^{Cl}**1**	26
^{H}**1** (ref. 21)	65
^{Me}**1**	83
^{OMe}**1**	126
^{naph}**1**	54
[Sn(C$_6$H$_4$(NMe)$_2$)]	222[a]
[Sn(C$_6$H$_4$(NCH$_2$Ch$_2$OMe)$_2$)]	148[a]
[Sn(C$_6$H$_4$(NCH$_2$CH$_2$CH$_2$N(Me)$_2$)$_2$)]	52[a]

[a] Ref. 26.

the coordination number of the tin center.[29,48] The appearance of a ^{119}Sn signal in a higher magnetic field region indicates the presence of a four-coordinate tin(II) complex, whereas a ^{119}Sn signal appearing in a lower magnetic field region indicates formation of a two-coordinate tin(II) center.[31,35] For example, two-coordinate monomeric stannylene, [Sn(C$_6$H$_4$(NMe)$_2$)], existing in a diluted C$_6$D$_6$ solution, exhibits a ^{119}Sn signal at 222 ppm.[26] A tin(II) complex, [Sn(C$_6$H$_4$(NCH$_2$Ch$_2$OMe)$_2$)], which exhibits a monomer structure with weak intramolecular interactions between the tin(II) centre and the two ether oxygen atoms of the ligand sidearm, shows a ^{119}Sn signal at 148 ppm.[26] On the other hand, a dimer complex, [Sn(C$_6$H$_4$(NCH$_2$CH$_2$CH$_2$N(Me)$_2$)$_2$)]$_2$, consisting of intramolecular Sn–NMe$_2$ interactions and intermolecular Sn–N (phenylenediamido of a neighboring molecule) interactions, affords four-coordinated tin(II) centres, which show a ^{119}Sn signal at 52 ppm.[26] The ^{119}Sn chemical shifts of the series of ^{R}**1** complexes varied from 26 to 126 ppm. Since all the complexes adopt a four-coordinate monomer structure in the solid state as revealed by the crystallographic study (Fig. 3), the observed variation of the ^{119}Sn chemical shift suggests involvement of an equilibrium between the three and/or four-coordinate structure and its two-coordinate one that is formed by dissociation of the coordinating solvent molecules, as shown in eqn (1):

$$[\mathrm{Sn}(^{R}\mathrm{L}^{TIPT})(\mathrm{solvent})_2] \rightleftarrows [\mathrm{Sn}(^{R}\mathrm{L}^{TIPT})(\mathrm{solvent})] + \mathrm{solvent} \rightleftarrows [\mathrm{Sn}(^{R}\mathrm{L}^{TIPT})] + 2\,\mathrm{solvent} \quad (1)$$

The ^{119}Sn signal of ^{Cl}**1** appeared at the highest magnetic field among the series of ^{R}**1** complexes, suggesting that 2p$_z$ (2N of *o*-phenylenediamido) → 5p$_z$ (Sn) donation was weakened by the electron-withdrawing chloro-substituents, making dissociation of the coordinating solvent molecules from the tin(II) centre difficult in C$_6$D$_6$. Thus, the four-coordinate tin(II) centre in ^{Cl}**1** is more stabilized. On the other hand, ^{OMe}**1** had its ^{119}Sn peak at the lowest magnetic field due to the electron-donating nature of the methoxy substituents, making the equilibrium proceed in the right-arrow direction of eqn (1). In fact, the ^{1}H NMR spectrum of ^{OMe}**1** in C$_6$D$_6$ showed ^{1}H signals assignable to a free THF molecule (dissociated THF) in solution. Judging from the observed ^{119}Sn chemical shifts, it can be concluded that the solvent-coordinated complexes are

more stabilized as the substituent R goes from OMe, Me, H, naph and to Cl.

Effects of the bulky TIPT substituent on stability toward hydrolysis

As revealed by the crystal structure analysis of ^{R}**1**, the TIPT substituents effectively stabilise the monomer tin(II) structure and allow coordination of two solvent molecules. Since stannylene is known to undergo hydrolysis easily,[31] the stability of ^{H}**1** toward hydrolysis was compared to that of **SnL**$^{Ph(tBu)2}$ and **SnL**^{Ph}. Addition of a small amount of water to a THF solution of each complex resulted in the formation of original ligand precursors, $^{H}LH_2$ and a white powder of SnO according to eqn (2):

$$[Sn(^{H}L)] + H_2O \xrightarrow[THF]{} SnO + {}^{H}LH_2 \quad (2)$$

In Fig. 4(a), the spectral changes for the hydrolysis of ^{H}**1** are shown. The absorption band of ^{H}**1** at 330 nm decreases with the increasing absorption band at 300 nm due to the original ligand with an isosbestic point at 325 nm, obeying first-order kinetics (see inset of Fig. 4(a)). The pseudo-first-order rate constant (k_{obs}, s^{-1}) was proportional to the concentration of added water, as shown in Fig. 4(b), from which the second-order rate constant (k) was obtained as 2.4 M^{-1} s^{-1}. The hydrolytic reactions of **SnL**$^{Ph(tBu)2}$ and **SnL**^{Ph} were analyzed in a similar manner to that of ^{H}**1**, and the second-order rate constants were determined as 26 M^{-1} s^{-1} and 54 M^{-1} s^{-1}, respectively (Fig. 4(b)). The second-order rate constants of **SnL**$^{Ph(tBu)2}$ and **SnL**^{Ph} are larger by about 10 and 22 times, respectively, than that of ^{H}**1**, demonstrating that both of the bulky TIPT substituents and the coordinating solvent molecules suppress the attack of water molecules at the tin(II) centre.

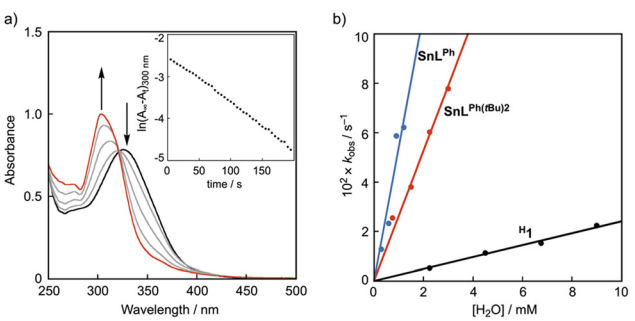

Fig. 4 (a) Time-dependent UV-vis spectral changes of a THF solution of ^{H}**1** in the presence of H_2O (0.03 mM). The inset shows the pseudo-first-order plot based on the absorbance change at 300 nm. (b) Plots of k_{obs} (s^{-1}) against [H_2O] (black: ^{H}**1**, red: **SnL**$^{Ph(tBu)2}$, blue: **SnL**^{Ph}).

Electrochemical properties of the tin(II) complexes

We recently reported electrochemical properties of ^{H}**1** in THF, which was the first example of one of the tin(II) complexes with *o*-phenylenediamido ligands to be subjected to CV measurement.[23] In this study, substituent effects of ^{R}**1** on electrochemical properties of ^{Cl}**1**, ^{Me}**1**, ^{OMe}**1**, and ^{naph}**1** were also

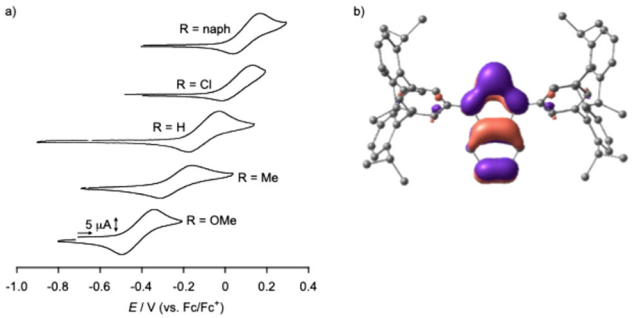

Fig. 5 (a) Cyclic voltammograms of ^{R}**1** and ^{naph}**1** in THF. (b) Frontier Kohn–Sham orbital of the HOMO for ^{H}**1** (B3LYP/SDD (for Sn), D95** (for the other atoms)). In the calculation, the coordinating THF molecules were omitted.

examined. As shown in Fig. 5(a), a quasi-reversible redox wave was observed at +0.05 V, −0.10 V, −0.24 V, and −0.45 V *vs.* Fc/Fc^+, respectively. ^{naph}**1** also exhibited a quasi-reversible redox wave at +0.13 V *vs.* Fc/Fc^+. Apparently, the oxidation potential of the tin(II) complexes shifts toward the negative direction as the electron-donating nature of the substituent of ^{R}**1** increases from Cl, H, Me, to OMe. We have already demonstrated that one-electron oxidation of ^{H}**1** takes place at the supporting ligand to generate the diiminosemiquinone radical complex of tin(II), ^{R}**2**.[23] The observed substituent-dependent negative shift of the oxidation potential further supports this conclusion. Fig. 5(b) shows the HOMO diagram of ^{H}**1** obtained by DFT calculations, where the majority of the HOMO exists on the phenylenediamido moiety. In both CVs of **SnL**$^{Ph(tBu)2}$ and **SnL**^{Ph}, irreversible oxidation waves were observed at E_{pa} = −0.20 V and E_{pa} = −0.17 V, respectively.

Reactivity of the tin(II) complexes toward organic azides

The reactivity of ^{R}**1** complexes in a C–H amination reaction was examined using trisylazide (N_3–Trs) as a substrate (Fig. 2 and Scheme 1). Following the reactions of ^{OMe}**1**, ^{Me}**1** and ^{H}**1**, sultam (5,7-diisopropyl-2,3-dihydro-3,3-dimethyl-1,2-benzothiazole-1,1-dioxide) was obtained in 25, 23 and 22% yields, respectively. As a by-product, trisylamine was also obtained. However, sultam was not obtained from the reactions of trisylazide with ^{Cl}**1** and ^{naph}**1**. Such a difference in the reactivity can be attributed to whether the nitrene-radical bound species, [Sn(^{R}L)(Trs–N$^{\bullet}$)] (^{R}**2**$^{Trs–N\bullet}$), is generated as the reactive oxidant by electron transfer from the *o*-phenylenediamido

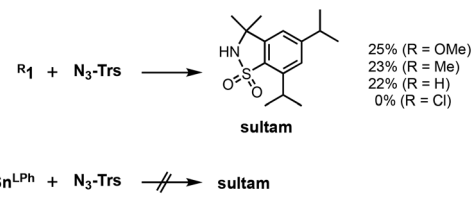

Scheme 1 Reactivity differences of tin(II) complexes in the C–H amination.

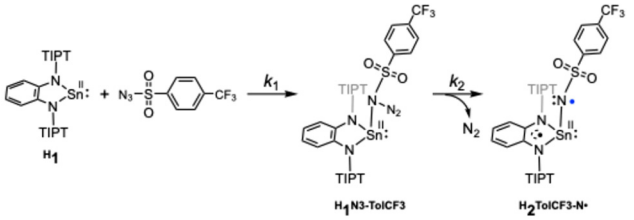

Scheme 2 Formation mechanism of $^{H}\mathbf{2}^{TolCF3-N\bullet}$ in the reaction of $^{H}\mathbf{1}$ and N_3–$TolCF_3$.

moiety to the bound N_3-Trs and the successive release of dinitrogen (N_2) (Scheme 2). In our previous paper, such a nitrene-radical bound species, $^{R}\mathbf{2}^{Trs-N\bullet}$, has been revealed as the active oxidant for the intramolecular amination reaction to give sultam.[23] In $^{R}\mathbf{2}^{Trs-N\bullet}$, most of the spin is located on the nitrene nitrogen atom (the spin density = 82%) while the remainder is on the tin(II) center (2%) and on the sulfonyl group (–$S(O)_2$–) (16%). Reactions of N_3-Trs with tin(II) complexes with sterically less hindered ligands, $\mathbf{SnL}^{Ph(tBu)2}$ and $\mathbf{SnL}^{Ph}$, did not give sultam.

Then, the reactivity of the tin(II) complexes toward organic azides was followed by UV-vis-NIR spectroscopy at low temperature. Since the nitrene-radical complex, $^{H}\mathbf{2}^{Ns-N\bullet}$, has a diiminosemiquinone radical unit, which exhibits a broad absorption band (960 nm) in the near-IR region,[23] formation of the analogues intermediate, $^{R}\mathbf{2}^{R'-N\bullet}$, was examined in the reactions of the series of $^{R}\mathbf{1}$ complexes and organic azides (N_3–R′) by monitoring the appearance of the broad absorption band in the near-IR region. Table S3† lists the λ_{max} of the near-IR absorption bands of the generated $^{R}\mathbf{2}^{R'-N\bullet}$. The absorption spectra of $^{R}\mathbf{2}^{R'-N\bullet}$ are given in Fig. S6.† Complex $^{OMe}\mathbf{1}$ activated all organic azides employed, N_3–R′, to produce a series of $^{R}\mathbf{2}^{R'-N\bullet}$. $^{Me}\mathbf{1}$ gave $^{Me}\mathbf{2}^{Ns-N\bullet}$, $^{Me}\mathbf{2}^{TolCF3-N\bullet}$ and $^{Me}\mathbf{2}^{Ts-N\bullet}$ from the reactions with the corresponding azides. Reactions of $^{H}\mathbf{1}$ with N_3–Ns and N_3–$TolCF_3$ also afforded $^{H}\mathbf{2}^{Ns-N\bullet}$ and $^{H}\mathbf{2}^{TolCF3-N\bullet}$, respectively. Reactions of other combinations did not proceed. Thus, the reactivity of $^{R}\mathbf{1}$ toward organic azides, N_3–R′, became higher as the oxidation potential became more negative: Cl → H → Me → OMe. Namely, $^{OMe}\mathbf{1}$ having the lowest oxidation potential exhibits the highest reactivity in the activation of organic azides. On the other hand, $^{Cl}\mathbf{1}$ and $^{naph}\mathbf{1}$ having higher oxidation potentials did not reduce the azides. IR spectra of the organic azides were recorded to observe the $\nu_{N\equiv N}$ stretch bands and their values are also listed in Table S3.† As is clearly seen, the higher the $\nu_{N\equiv N}$ value, the easier the dinitrogen release.

It is proposed that generation of a nitrene bound metal complex $^{R}\mathbf{2}^{R'-N\bullet}$ from the precursor complex $^{R}\mathbf{1}$ and an organic azide N_3–R′ requires the following two steps: (1) coordination of an organic azide to the precursor complex to yield an adduct complex and (2) elimination of a dinitrogen molecule (N_2) from the adduct complex. A large number of nitrene bound metal complexes including metal imido and metal nitrene-radical complexes have so far been prepared by such reactions. However, no kinetics study on such a two-step process has been reported. By careful inspection of the absorption spectral change of $^{R}\mathbf{1}$ observed upon addition of N_3–R′, we found that the reaction of $^{H}\mathbf{1}$ with N_3–$TolCF_3$ giving $^{H}\mathbf{2}^{TolCF3-N\bullet}$ consisted of two-step processes. Fig. 6(a) shows spectral changes for the reaction of $^{H}\mathbf{1}$ (1.0 mM) in the presence of N_3–$TolCF_3$ (20.0 mM) in toluene at −40 °C. The original spectrum (black line) of $^{H}\mathbf{1}$ readily changed to the red line spectrum, and then the characteristic absorption bands at 490, 880, and 965 nm due to the nitrene-radical bound complex, $^{H}\mathbf{2}^{TolCF3-N\bullet}$, gradually appeared (green line spectrum) (Fig. S7†). The time course of the absorbance changes at 455 nm was fitted by using eqn (3), from which the apparent rate constants for the first step, k_{obs1} (s^{-1}), and the second step, k_{obs2} (s^{-1}), were obtained (Fig. 6(b)):

$$\mathrm{Abs}_{455} = a + b \cdot \exp(-k_{obs1} \cdot t) - c \cdot \exp(-k_{obs2} \cdot t) \quad (3)$$

As shown in Fig. 6(c) and (d), k_{obs1} (s^{-1}) was proportional to the concentration of N_3–$TolCF_3$, whereas k_{obs2} (s^{-1}) was independent of N_3–$TolCF_3$ concentration, from which the second-order rate constant k_1 and the first-order rate constant k_2 were determined as being 0.19 M^{-1} s^{-1} and 5×10^{-3} s^{-1}, respectively (the time courses of the absorbance changes at each concentration of N_3–$TolCF_3$ are given in Fig. S8†). The first step is safely assigned to that involving coordination of N_3–$TolCF_3$ to $^{H}\mathbf{1}$ to yield an intermediate $^{H}\mathbf{1}^{N3-TolCF3}$, while the second step involves N_2 elimination from $^{H}\mathbf{1}^{N3-TolCF3}$ coupled with a one-electron transfer from the phenylenediamido moiety to the

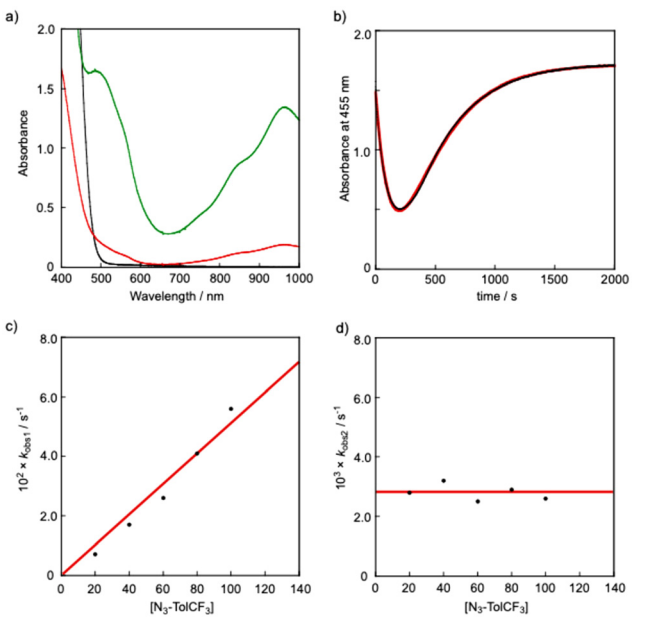

Fig. 6 (a) Spectral changes observed upon addition of N_3–$TolCF_3$ (20.0 mM) to $^{H}\mathbf{1}$ (1.0 mM) in toluene at −40 °C: $^{H}\mathbf{1}$ (black) → $^{H}\mathbf{1}^{N3-TolCF3}$ (red) → $^{H}\mathbf{2}^{TolCF3-N\bullet}$ (green). (b) Time course of the absorbance change at 455 nm (black). Simulation of the time course (red): $Abs_{455} = a + b{\cdot}\exp(-k_{obs1}{\cdot}t) + c{\cdot}\exp(-k_{obs2}{\cdot}t)$; a = 1.7, b = 3.4, k_{obs1} = 7.1 × 10^{-3}, c = −3.6, k_{obs2} = 2.8 × 10^{-3}, R^2 = 0.9996. (c) Plot of k_{obs1} against [N_3–$TolCF_3$]. (d) Plot of k_{obs2} against [N_3–$TolCF_3$].

azide moiety to give $^{H}2^{TolCF3-N\bullet}$ (Scheme 2). On the other hand, when $^{OMe}1$ was employed instead of $^{H}1$, the UV-vis spectrum of $^{OMe}1$ was directly changed to that of $^{OMe}2^{TolCF3-N\bullet}$ following a single exponential kinetics equation, namely the adduct intermediate was not detected spectroscopically (Fig. S9†). Such a difference in the kinetics behaviors can be explained as follows. The oxidation potential of $^{H}1$ is higher than that of $^{OMe}1$. Thus, the intramolecular electron transfer from the phenylenediamido unit to the coordinating azide in $^{H}1^{N3-TolCF3}$ must be slower than that in the methoxy analogue $^{OMe}1^{N3-TolCF3}$. Accordingly, the first step for adduct formation of N_3–$TolCF_3$ and $^{H}1$ was observable. On the other hand, intramolecular electron transfer within $^{OMe}1^{N3-TolCF3}$ to produce $^{OMe}2^{TolCF3-N\bullet}$ will be much faster than that within $^{H}1^{N3-TolCF3}$ taking the lower oxidation potential of $^{OMe}1$ into account. Moreover, the tin(II) centre of $^{OMe}1$ favors the two-coordinate structure as revealed by the ^{119}Sn NMR spectral examination (Table 1), where the initial association process between $^{OMe}1$ and N_3–$TolCF_3$, namely coordination of N_3–$TolCF_3$ to $^{OMe}1$, becomes unfavorable (slower) when compared with the case of $^{H}1$.

The formation mechanism of $^{H}2^{TolCF3-N\bullet}$ deduced by the kinetics study is further supported by DFT calculations. The majority of the LUMO of $^{H}1$ comprises the $5p_z$ orbital of the tin(II) centre as shown in Fig. S10,† which accepts coordination of N_3–$TolCF_3$ to yield the adduct complex, $^{H}1^{N3-TolCF3}$. This complex adopts the closed-shell singlet state (CSS), where the phenylenediamido unit constitutes the HOMO whereas the N_3–$TolCF_3$ part significantly contributes to the LUMO (Fig. 7). The energy difference between the HOMO and LUMO of $^{H}1^{N3-TolCF3}$ is 2.41 eV. In the conversion of $^{H}1^{N3-TolCF3}$ to $^{H}2^{TolCF3-N\bullet}$, the transition state (TS) is also a CSS, which is formed with E_a = 10.5 kcal mol^{-1}. Two electrons in the HOMO of the TS delocalize over the phenylenediamido and N_3–$S(O)_2$– units excluding the sulfur and tin atoms and similarly in the LUMO there are contributions from the two units. Following the dinitrogen elimination with ΔE = −16.0 kcal mol^{-1}, a triplet state is generated in the nitrene-radical bound complex $^{H}2^{TolCF3-N\bullet}$ having a triplet state is generated.

To confirm that $^{H}2^{TolCF3-N\bullet}$ is a triplet species, its X-band electron paramagnetic resonance (EPR) spectrum was recorded in toluene glass at 4.1 K (Fig. 8). As observed in $^{H}2^{Ns-N\bullet}$, which was recently reported,[23] the half-field transition for ΔM_S = ±2

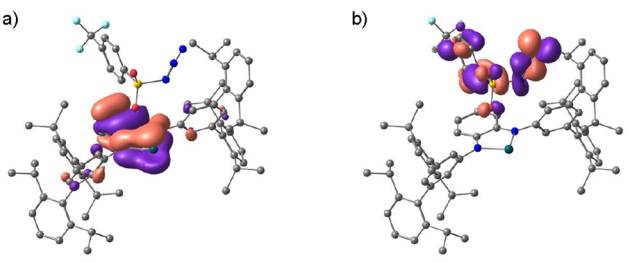

Fig. 7 (a) Frontier Kohn–Sham orbitals of the HOMO (a) and the LUMO (b) for $^{H}1^{N3-TolCF3}$ (B3LYP/SDD (for Sn), D95** (for the other atoms)).

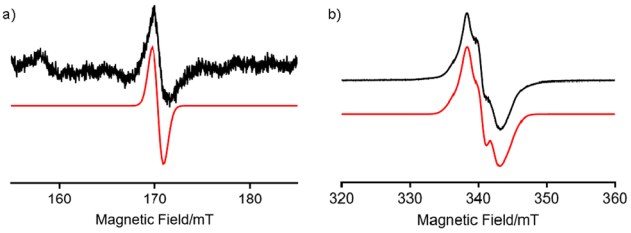

Fig. 8 EPR spectra of $^{H}2^{N\bullet TolCF3}$ observed in toluene glass at 4.1 K. (a) A half-field EPR transition of $^{H}2^{TolCF3-N\bullet}$. (b) Allowed EPR transitions. The observed spectrum (black) is compared with a simulated one (red) including a radical impurity. The signal intensity of the half-field transitions was two-orders of magnitude smaller than that of the allowed transitions.

was observed at $g \sim 4$ together with allowed transitions for ΔM_S = ±1, demonstrating that $^{H}2^{TolCF3-N\bullet}$ also includes a spin-triplet species. By simulating the observed spectra using the Easyspin toolbox[40] on MATLAB software, we determined magnetic parameters of $^{H}2^{N\bullet-TolCF3}$ as follows: g_{xx} = 2.001, g_{yy} = 1.998, g_{zz} = 2.000, $|D|$ = 0.0039 cm^{-1}, and $|E|$ = 0.0005 cm^{-1}. The signal intensities of the half-field transitions were not proportional to $1/T$, indicating that the spin-triplet species is in a thermally excited state (Fig. S11†). Thus, this triplet species was characterised as a tin(II)–nitrene-radical complex with a diiminobenzosemiquinone radical anion, $^{H}2^{TolCF3-N\bullet}$.

Conclusions

In this manuscript, tin(II) complexes with *o*-phenylenediamido ligands that have a terphenyl-based sterically bulky substituent were synthesised and then characterised by several spectroscopic methods. Crystal structures of all complexes were determined and these show tin(II) centres that adopt a four-coordinate structure with two amido nitrogen atoms of the *o*-phenylenediamido ligand and two solvent molecules. Following ^{119}Sn NMR study of the complexes in C_6D_6, each tin(II) center was revealed to exist in equilibrium between the four-coordinate tin(II) centre and the two-coordinate version formed by dissociation of the two solvent ligands, where ligands having electron-donating groups stabilised the two-coordinate tin(II) centre while those having electron-withdrawing groups stabilised the four-coordinate species. The terphenyl-based bulky substituent stabilised the tin(II) centre against hydrolysis, which was demonstrated by comparing its stability with that of the tin(II) complexes with less bulky substituents. The tin(II) complexes with sterically demanding *o*-phenylenediamido-based ligand derivatives underwent ligand-based redox and the oxidation potential varied from −0.45 V to +0.13 V as the substituent goes from –OMe to –naph. The tin(II) complexes having electron-donating groups exhibited intramolecular C–H amination of trisylazide to give sultam but the amination product was not obtained by the reactions of those complexes having electron-withdrawing groups with this substrate. Such a difference in the reactivity was the availability of the nitrene-

radical bound tin(II) reactive intermediate. A step of binding an organic azide to a tin(II) complex and then successive one-electron transfer steps from the ligand to the bound azide moiety to give the nitrene radical tin(II) complex were analyzed kinetically. The combination of the *o*-phenylenediamido ligands and a tin(II) centre provides further insights into the roles of redox-active ligands in the reactions of main group element complexes.

Experimental

Materials and methods

General

Reagents and solvents used in this study except for the ligand and complexes were commercial products of the highest available purity. The solvents were stored with a molecular sieve 4A. Silica gel 60 (0.063–0.200 mm) made by Merck was used for silica gel column chromatography. $Sn[N(SiMe_3)_2]_2$,[36] [Sn(L^{Ph})][29] and [Sn($^{H}L^{TIPT}$)] (**^{H}1**)[23] were prepared according to reported methods under argon in a Miwa DB0-1KP glovebox. $L^{Ph(tBu)2}H_2$,[15] 5′-bromo-2,4,2″,4″-tetraisopropyl-[1,1′:3′,1″]terphenyl (TIPT-Br),[23] 4,5-dimethoxyphenylene-1,2-diamine,[37] 4-methylbenzenesulfonyl azide (N_3–Ts),[38] 4-nitrobenzenesulfonyl azide (N_3–Ns),[38] 4-(trifluoromethyl)benzenesulfonyl azide (N_3–TolCF$_3$),[39] 2,4,6-trimethylphenylazide (N_3–Mes),[40] 1-azido-4-nitrobenzene (N_3–PhNO$_2$)[40] and mestylazide[41] were synthesised by following the reported methods. EPR measurements were carried out on a BRUKER ELEXSYS E600 spectrometer under non-saturating microwave power conditions. UV-vis spectra were recorded on a Hewlett Packard 8453 photodiode array spectrophotometer equipped with a UNISOK thermostated cell holder (USP-203). Solution IR spectra were acquired on a SHIMAZU spectrometer (IRPrestige-21). ^{1}H, ^{13}C and ^{119}Sn NMR spectra were recorded on a JEOL ECP 400 or a JEOL ECS 400 spectrometer. Elemental analysis and HR-MS measurements were conducted in the Analytical Instrumentation Center of the Graduate School of Engineering, Osaka University. Electrochemical measurements were performed using a KOREA KIYON KK-011AS glovebox with a Hokuto Denko HZ-7000 in THF (1.0 mM) containing ^{n}Bu$_4$NPF$_6$ (0.1 M) at room temperature. A set of a carbon working electrode (diameter = 3 mm), an Ag/AgNO$_3$/CH$_3$CN reference electrode and a platinum counter electrode was employed in these experiments. All redox potentials are referenced to the ferrocene/ferrocenium (Fc/Fc$^+$) redox potential. The values of $E_{1/2}$ and $\Delta(E_{pa} - E_{pc})$ *vs.* Ag/AgNO$_3$ from the cyclic voltammogram of Fc were 0.30 V and 0.20 V, respectively, under the employed conditions.

***N*,*N*′-Bis[2,6,2″,6″-tetra-isopropyl-*m*-terphenyl]-4,5-dichlorophenylene-1,2-diamine (^{Cl}LH$_2$).** 4,5-Dichlorophenylene-1,2-diamine (354 mg, 2.00 mmol), TIPT–Br (1.91 g, 4.00 mmol) and NaO^{t}Bu (576 mg, 6.00 mmol) were placed in a 100 mL three-neck flask with a magnetic bar stirrer. $Pd_2(dba)_3$ (91.6 mg, 0.100 mmol), *rac*-BINAP (93.4 mg, 0.150 mmol) and toluene (5.0 mL) were added to a 50 mL eggplant flask under an N_2 atmosphere. After stirring the solution for 6 h, the generated [Pd(binap)] catalyst solution was added by cannulation into the 100 mL three–neck flask previously prepared. The mixture was heated to 110 °C and stirred overnight at this temperature. The resultant suspension was cooled to room temperature. Insoluble material was removed by filtration through a pad of Celite and the solid was washed with CH_2Cl_2 until the filtrate became colorless. The combined filtrate was concentrated under reduced pressure to give a crude product of $^{Cl}L^{TIPT}H_2$, which was purified by silica gel column chromatography using a mixed solvent of hexane/chloroform (v/v = 3 : 1) as an eluent. A pale-yellow band was collected and evaporated to give a white solid of $^{Cl}L^{TIPT}H_2$ (891 mg, 46%), which was recrystallized by slow diffusion of acetonitrile into a THF solution. Anal. calcd (%) for $C_{66}H_{76}Cl_2N_2$·0.3THF: C, 81.37; H, 8.17; N, 2.82. Found: C, 81.42; H, 8.10; N, 2.84. ^{1}H NMR (CDCl$_3$, 600 MHz, ppm): δ = 7.41 (s, 2H, H_{ArN_2}), 7.32 (t, J = 7.8 Hz, 4H, H_{TIPT}), 7.18 (d, J = 7.8 Hz, 8H, H_{TIPT}), 6.83 (d, J = 1.2 Hz, 4H, H_{TIPT}), 6.64 (t, J = 1.2 Hz, 2H, H_{TIPT}), 5.69 (s, 2H, H_{NH}), 2.81 (sep, J = 7.2 Hz, 8H, $H_{CH(iPr)}$), 1.17 (d, J = 7.2 Hz, 24H, $H_{Me(iPr)}$), 1.08 (d, 7.2 Hz, 24H, $H_{Me(iPr)}$). ^{13}C NMR (CDCl$_3$, 600 MHz, ppm): δ = 146.57, 142.00, 138.68, 134.60, 127.90, 125.04, 124.88, 122.50, 119.58, 117.53, 30.46, 24.40, 24.19 (Fig. S1†). HR-MS (FAB$^+$): m/z = 968.5540.

[Sn(^{Cl}L)(THF)$_2$] (^{Cl}1). To a THF (1.0 mL) solution containing $^{Cl}LH_2$ (0.400 mmol, 387 mg) was added $Sn[N(SiMe_3)_2]_2$ (0.404 mmol, 177 mg) under an argon atmosphere. The reaction mixture was then stirred for 36 h at ambient temperature to yield yellow powder, which was collected by filtration (199 mg, 46%). Anal. calcd (%) for $C_{66}H_{76}Cl_2N_2Sn$·2THF·2.8H_2O: C, 69.35; H, 7.68; N, 2.19. Found: C, 69.32; H, 7.52 N, 2.19. ^{1}H NMR (C_6D_6, 600 MHz, ppm): δ = 7.59 (s, 2H, H_{ArN_2}), 7.33 (t, J = 7.8 Hz, 4H, H_{TIPT}), 7.22 (d, J = 7.8 Hz, 8H, H_{TIPT}), 6.90 (s, 4H, H_{TIPT}), 6.54 (s, 2H, H_{TIPT}), 3.47 (m, 8H, H_{THF}), 3.15 (sep, J = 6.6 Hz, 8H, $H_{CH(iPr)}$), 1.33 (m, 4H, H_{THF}), 1.29 (d, J = 6.6 Hz, 24H, $H_{Me(iPr)}$), 1.23 (d, J = 6.6 Hz, 24H, $H_{Me(iPr)}$). ^{13}C NMR (C_6D_6, 600 MHz, ppm): δ = 146.81, 145.74, 144.28, 142.87, 139.30, 128.65, 127.15, 123.35, 123.04, 116.88, 112.92, 67.89, 31.05, 25.69, 24.76, 24.68. ^{119}Sn NMR (C_6D_6, 600 MHz): δ = 26.2 ppm.

***N*,*N*′-Bis[2,6,2″,6″-tetra-isopropyl-*m*-terphenyl]-4,5-dimethylphenylene-1,2-diamine (^{Me}LH$_2$).** This ligand was prepared in a similar manner to that for the synthesis of $^{Cl}LH_2$ by using 4,5-dimethylphenylene-1,2-diamine (272 mg, 2.00 mmol) instead of 4,5-dichlorophenylene-1,2-diamine. A white solid sample of $^{Me}LH_2$ (1.10 g, 59%) was obtained after purification by silica gel column chromatography using a mixed solvent of hexane/chloroform (v/v = 3 : 1) as an eluent. $^{Me}LH_2$ was recrystallized by slow diffusion of acetonitrile into a THF solution. Anal. calcd (%) for $C_{68}H_{82}N_2$·0.3THF: C, 87.39; H, 9.16; N, 2.95. Found: C, 87.34; H, 9.17; N, 2.95. ^{1}H NMR (CDCl$_3$, 600 MHz, ppm): δ = 7.30 (t, J = 7.2 Hz, 4H, H_{TIPT}), 7.19 (s, 2H, H_{ArN_2}), 7.17 (d, J = 7.2 Hz, 8H, H_{TIPT}), 6.77 (d, J = 1.8 Hz, 4H, H_{TIPT}), 6.51 (t, J = 1.2 Hz, 2H, H_{TIPT}), 5.62 (s, 2H, H_{NH}), 2.85 (sep, J = 7.2 Hz, 8H, $H_{CH(iPr)}$), 1.16 (d, J = 7.2 Hz, 24H, $H_{Me(iPr)}$), 1.07 (d, 7.2 Hz, 24H, $H_{Me(iPr)}$). ^{13}C NMR (CDCl$_3$, 600 MHz, ppm): δ =

146.63, 143.78, 141.48, 139.24, 132.36, 130.84, 127.67, 123.14, 122.41, 121.04, 116.16, 30.37, 24.43, 24.20, 19.26 (Fig. S2†). HR-MS (FAB^+): m/z = 928.6641.

[Sn(^{Me}L)(THF)(CH_3CN)] (^{Me}1). This compound was prepared in a similar manner to that for the synthesis of ^{Cl}**1** by using $^{Me}LH_2$ (371 mg, 0.400 mmol) instead of $^{Cl}LH_2$ and isolated as a yellow powder (293 mg, 70%). Anal. calcd (%) for $C_{68}H_{82}N_2Sn{\cdot}2.2THF{\cdot}1.5H_2O$: C, 74.89; H, 8.40; N, 2.27. Found: C, 74.78; H, 8.42 N, 2.36. ^{1}H NMR (C_6D_6, 600 MHz, ppm): δ = 7.49 (s, 2H, H_{ArN_2}), 7.35 (t, J = 7.8 Hz, 4H, H_{TIPT}), 7.24 (d, J = 7.8 Hz, 8H, H_{TIPT}), 6.89 (s, 4H, H_{TIPT}), 6.61 (s, 2H, H_{TIPT}), 3.54 (m, 8H, H_{THF}), 3.23 (sep, J = 6.6 Hz, 8H, $H_{CH(iPr)}$), 1.39 (m, 4H, H_{THF}), 1.27 (d, J = 6.6 Hz, 24H, $H_{Me(iPr)}$), 1.26 (d, J = 6.8 Hz, 24H, $H_{Me(iPr)}$). ^{13}C NMR (C_6D_6, 600 MHz, ppm): δ = 146.87, 146.74, 142.51, 142.43, 139.71, 128.35, 126.44, 125.93, 123.38, 122.99, 114.16, 67.85, 30.99, 25.78, 24.82, 24.68. ^{119}Sn NMR (C_6D_6, 600 MHz): δ = 83.3 ppm.

***N*,*N*′-Bis[2,6,2″,6″-tetra-isopropyl-*m*-terphenyl]-4,5-dimethoxyphenylene-1,2-diamine (^{OMe}LH$_2$).** This ligand was prepared in a similar manner to that for the synthesis of $^{Cl}LH_2$ by using 4,5-dimethoxyphenylene-1,2-diamine (252 mg, 1.50 mmol) instead of 4,5-dichlorophenylene-1,2-diamine. A light orange solid sample of $^{OMe}LH_2$ (1.10 g, 59%) was obtained after purification by silica gel column chromatography using a mixed solvent of hexane/chloroform (v/v = 1 : 2) as an eluent. The obtained solid was washed with acetonitrile to give a white solid of $^{OMe}LH_2$ (0.58 g, 40%). Anal. calcd (%) for $C_{68}H_{84}N_2O_2{\cdot}2.5H_2O$: C, 81.14; H, 8.91; N, 2.78. Found: C, 81.14; H, 8.60; N, 2.85. ^{1}H NMR ($CDCl_3$, 400 MHz, ppm): δ = 7.30 (t, 4H, H_{TIPT}), 7.16 (d, 8H, H_{TIPT}), 6.93 (s, 2H, H_{ArN_2}), 6.69 (d, J = 1.2, 2H, H_{TIPT}), 6.50 (t, J = 1.2 Hz, 4H, H_{TIPT}), 5.63 (s, 2H, H_{NH}), 3.75 (s, 6H, H_{OMe}), 2.82 (sept, J = 6.6 Hz, 8H, $H_{CH(iPr)}$), 1.12 (d, J = 6.6 Hz, 24H, $H_{Me(iPr)}$), 1.05 (d, J = 6.6 Hz, 24H, $H_{Me(iPr)}$). ^{13}C NMR ($CDCl_3$, 600 MHz, ppm): δ = 146.54, 145.39, 144.30, 141.58, 139.21, 128.22, 127.72, 123.24, 122.42, 115.48, 106.48, 56.37, 30.34, 24.44, 24.14 (Fig. S3†). HR-MS (FAB^+): m/z = 960.6554.

[Sn(^{OMe}L)(THF)(CH_3CN)] (^{OMe}1). This compound was prepared in a similar manner to that for the synthesis of ^{Cl}**1** by using $^{OMe}LH_2$ (0.400 mmol, 371 mg) instead of $^{Cl}LH_2$ and was isolated as a yellow powder (293 mg, 70%), which was recrystallized by slow diffusion of acetonitrile into a THF solution. Anal. calcd (%) for $C_{68}H_{82}N_2O_2Sn{\cdot}THF{\cdot}CH_3CN{\cdot}0.5H_2O$: C, 74.05; H, 7.89; N, 3.50. Found: C, 73.85; H, 8.15 N, 3.68. ^{1}H NMR (C_6D_6, 600 MHz, ppm): δ = 7.34 (t, J = 7.8 Hz, 4H, H_{TIPT}), 7.28 (d, J = 1.8 Hz, 4H, H_{TIPT}), 7.23 (s, 2H, H_{ArN_2}), 7.23 (d, J = 7.8 Hz, 8H, H_{TIPT}), 6.92 (s, 2H, H_{TIPT}), 3.62 (s, 6H, H_{OMe}), 3.53 (m, 2.5H, H_{THF}), 3.22 (dsep, J = 6.9, 0.6 Hz, 8H, $H_{CH(iPr)}$), 1.24 (dd, J = 6.9, 0.6 Hz, 48H, $H_{Me(iPr)}$). ^{13}C NMR (C_6D_6, 600 MHz, ppm): δ = 146.76, 146.22, 144.48, 142.47, 139.50, 138.97, 128.48, 127.30, 123.85, 122.94, 100.91, 57.74, 30.93, 24.82, 24.48. ^{119}Sn NMR (C_6D_6, 600 MHz): δ = 126 ppm.

***N*,*N*′-Bis[2,6,2″,6″-tetra-isopropyl-*m*-terphenyl]-naphthalene-2,3-diamine (^{naph}LH$_2$).** This ligand was prepared in a similar manner to that for the synthesis of $^{Cl}LH_2$ by using naphthalene-2,3-diamine (257 mg, 1.50 mmol), instead of 4,5-dichlorophenylene-1,2-diamine. A light orange solid sample was obtained by silica gel column chromatography using a mixed solvent of hexane/chloroform (v/v = 3 : 1) as an eluent, which was washed with acetonitrile to give a white solid of $^{naph}LH_2$ (0.78 g, 55%). Anal. calcd (%) for $C_{70}H_{82}N_2$: C, 88.37; H, 8.69; N, 2.94. Found: C, 88.22; H, 8.85; N, 2.90. ^{1}H NMR ($CDCl_3$, 400 MHz, ppm): δ = 7.77 (s, 2H, H_{ArN_2}), 7.48 (m, 2H, H_{ArN_2}), 7.32 (t, J = 7.6 Hz, 4H, H_{TIPT}), 7.23 (m, 2H, H_{ArN_2}), 7.20 (d, J = 7.6 Hz, 8H, H_{TIPT}), 6.98 (d, J = 1.2, 4H, H_{TIPT}), 6.30 (t, J = 1.2 2H, H_{TIPT}), 5.92 (s, 2H, H_{NH}), 2.88 (sep, J = 6.8 Hz, 8H, $H_{CH(iPr)}$), 1.20 (d, J = 6.8 Hz, 24H, $H_{Me(iPr)}$), 1.10 (d, J = 6.8 Hz, 24H, $H_{Me(iPr)}$). ^{13}C NMR ($CDCl_3$, 600 MHz, ppm): δ = 146.60, 142.71, 141.80, 138.96, 135.09, 129.96, 127.81, 126.12, 124.42, 124.36, 122.47, 117.53, 113.67, 30.45, 24.43, 24.24 (Fig. S4†). HR-MS (FAB^+): m/z = 950.6500.

[Sn(^{naph}L)(THF)$_2$] (^{naph}1). This compound was prepared in a similar manner to that for the synthesis of ^{Cl}**1** by using $^{naph}LH_2$ (0.404 mmol, 177 mg) instead of $^{Cl}LH_2$ and was isolated as a yellow powder (293 mg, 70%). The solid was recrystallized by slow diffusion of acetonitrile into a THF solution. Anal. calcd (%) for $C_{70}H_{80}N_2Sn{\cdot}1THF{\cdot}3H_2O$: C, 74.42; H, 7.93; N, 2.35. Found: C, 74.65; H, 7.99 N, 2.44. ^{1}H NMR (C_6D_6, 600 MHz, ppm): δ = 7.98 (s, 2H, H_{ArN_2}), 7.85 (m, 2H, H_{ArN_2}), 7.35 (s, 4H, H_{TIPT}), 7.34 (t, J = 7.8 Hz, 4H, H_{TIPT}), 7.25 (m, 2H, H_{ArN_2}), 7.24 (d, J = 7.8 Hz, 8H, H_{TIPT}), 6.93 (t, J = 1.2, 2H, H_{TIPT}), 3.53 (m, 2.5H, H_{THF}), 3.26 (dsep, J = 6.9, 0.6 Hz, 8H, $H_{CH(iPr)}$), 1.37 (m, 2.5H, H_{THF}), 1.31 (d, J = 6.6 Hz, 24H, $H_{Me(iPr)}$), 1.27 (d, J = 7.2 Hz, 24H, $H_{Me(iPr)}$). ^{13}C NMR (C_6D_6, 600 MHz, ppm): δ = 146.79, 145.66, 142.61, 139.58, 128.92, 128.48, 128.29, 126.47, 126.40, 123.33, 123.13, 122.97, 106.98, 30.97, 24.77, 24.68. ^{119}Sn NMR (C_6D_6, 600 MHz): δ = 54 ppm.

[Sn(L$^{Ph(tBu)2}$)(THF)] (SnL$^{Ph(tBu)2}$). This compound was prepared in a similar manner to that for the synthesis of ^{Cl}**1** by using $^{H}L^{PhtBu2}H_2$ (0.400 mmol, 194 mg) instead of $^{Cl}L^{TIPT}H_2$ and isolated as a yellow powder (216 mg, 90%). Anal. calcd (%) for $C_{34}H_{46}N_2Sn{\cdot}THF$: C, 67.76; H, 8.08; N, 4.16. Found: C, 67.99; H, 8.47 N, 4.16. ^{1}H NMR (THF-d_8, 600 MHz, ppm): δ = 7.39 (s, 4H, H_{Ph}), 7.31 (s, 2H, H_{Ph}), 7.17 (dd, J = 5.8 Hz, 3.4 Hz, 2H, H_{ArN_2}), 6.62 (dd, J = 5.8 Hz, 3.4 Hz, 2H, H_{ArN_2}), 1.53 (s, 36H, H_{Me}). ^{119}Sn NMR (C_6D_6, 600 MHz): δ = −58.0 ppm.

Kinetics study on the formation of tin–nitrenoid complexes

A toluene solution of ^{H}**1** (1.0 mM, 2.0 mL) in a 1.0 cm path-length UV-vis cuvette was held in a Unisoku thermostated cell holder at −40 °C. An aliquot (20 μL) of a toluene solution of N_3–$TolCF_3$ (1.0 g, 4.0 mmol in 1.0 mL) was added to the toluene solution of ^{H}**1** in the cuvette through a septum cap by using a gas-tight syringe to start the reaction. In this case, the molar ratio of ^{H}**1** and N_3–$TolCF_3$ was 1 : 20. The same procedures were repeated by changing the amount of added N_3–$TolCF_3$ (40, 60, 80, and 100 equiv. against ^{H}**1**). The reaction consisted of a two-step process: ^{H}**1** + N_3–$TolCF_3$ → [^{H}**1**$^{N3–TolCF3}$] → ^{H}**2**$^{TolCF3–N•}$. The time course of the absorbance changes at 455 nm due to the ^{H}**1**$^{N3–TolCF3}$ adduct intermediate was fitted by the following equation: Abs. = $a + b{\cdot}\exp(-k_{obs1}{\cdot}t) + c{\cdot}\exp(-k_{obs2}{\cdot}t)$ to give rate constants, where the apparent rate con-

stants, $k_{obs(1)}$ (s^{-1}) and $k_{obs(2)}$ (s^{-1}), correspond to the first step and the second step, respectively.

EPR measurement

An EPR sample tube (ϕ = 5 mm) containing a toluene solution (0.8 mL) of ^{H}**1** (1.0 mM) was cooled and kept at −40 °C with a dry ice-CH_3CN bath. To the toluene solution, a toluene solution of N_3–TolCF_3 was added through a septum cap by using a gas-tight syringe ([**1**] : [N_3–TolCF_3] = 1 : 1). After standing at −40 °C for 1 h to generate ^{H}**2**$^{TolCF3–N\bullet}$, the solution was frozen in liquid nitrogen. EPR spectra of the frozen solution were observed with an X-band ELEXSYS E600 EPR spectrometer (ν_{MW} = 9.5375 GHz) at liquid helium temperature. Microwave power of 0.01 mW and modulation amplitude of 0.1 mT were applied for the measurements of allowed transitions. On the other hand, microwave power of 1.0 mW and modulation amplitude of 1 mT were applied for the measurements of half-field forbidden transitions. The spectrum measured was simulated by the Easyspin toolbox.[42]

Intramolecular amination of trisylazide (N_3–Trs)

Trisylazide (35 μmol, 10.9 mg) was dissolved in toluene (1.0 mL) and then an aliquot (20 μL) of the solution was added to a toluene solution (1.0 mL) of ^{R}**1** (3.50 μmol), where the ratio of trisylazide : ^{R}**1** is 1 : 1. The mixture was stirred at 70 °C for 24 h under argon. All volatiles were evaporated *in vacuo* and the crude products were analyzed by ^{1}H NMR spectroscopy ($CDCl_3$, 400 MHz; internal standard: 1,4-dimethoxybenzene (2.07 mg, 15.0 μmol)). The aminated product (sultam: 5,7-diisopropyl-2,3-dihydro-3,3-dimethyl-1,2-benzothiazole-1,1-dioxide) was identified by comparing its ^{1}H NMR chemical shifts with those of the authentic sample.

X-ray crystallography. Single crystals of ^{Cl}**1**, ^{Me}**1**, ^{OMe}**1**, ^{naph}**1** and **SnL**$^{Ph(tBu)2}$ suitable for X-ray crystallographic analysis were obtained by slow diffusion of acetonitrile into the respective THF solution. Each single crystal was mounted on a loop with mineral oil. Data from X-ray diffraction patterns were recorded at −158 °C on a Rigaku R-AXIS RAPID diffractometer using filtered Mo-Kα radiation (0.71075 Å). The structures were resolved by direct methods (SHELXT)[43] and expanded using Fourier techniques. The non-hydrogen atoms were refined anisotropically by full-matrix least squares on F^2. The hydrogen atoms were attached at idealized positions on carbon atoms and were not refined. All calculations were performed using the program Olex2 crystallographic software packages.[44] For ^{Cl}**1**, one of the THF molecules coordinating toward the tin atom was disordered, and its hydrogen atoms were not attached to them. All structures in the final stage of refinement showed no movement in atom positions. There is no high-level alert in the check CIF file to the CIF and FCF files (https://checkcif.iucr.org). Crystallographic parameters are summarized in Table S1.† CCDC 2325047–2325051† contain the supplementary crystallographic data (CIF files) for ^{Cl}**1**, ^{Me}**1**, ^{OMe}**1**, ^{naph}**1** and **SnL**$^{Ph(tBu)2}$ reported in this paper.

Computational methodology. Energy calculations in the triplet, closed-shell singlet, and open-shell singlet states were performed using density functional theory implemented with the Gaussian16 program package.[45] The open-shell singlet state was computed using the broken-symmetry approach. Geometry optimizations were performed with the B3LYP functional.[46,47] For the Sn atom, the SDD basis set,[48,49] and for the other atoms, D95** basis set[50] were used.

Author contributions

H.S. conceived the idea and designed the project, and H.S. discussed all experimental results. A.Y. and M.Y. performed most of the experiments. K.S. contributed to EPR measurements and the analysis. Y.S., M.M. and K.Y. performed theoretical calculations. S.I. was involved in the discussion of experimental results. H.S. and S.I. wrote the manuscript. All the authors commented on the final draft of the manuscript and contributed to the analysis and interpretation of the data.

Data availability

All relevant data are within the manuscript and its ESI.†

Conflicts of interest

There are no conflicts to declare.

Acknowledgements

This work was supported by KAKENHI (Grant-in-Aid) for Scientific Research (No. 23K04767).

References

1 V. K. K. Praneeth, M. R. Ringenberg and T. R. Ward, *Angew. Chem., Int. Ed.*, 2012, **51**, 10228–10234.
2 O. R. Luca and R. H. Crabtree, *Chem. Soc. Rev.*, 2013, **42**, 1440–1459.
3 J. I. van der Vlugt, *Chem. – Eur. J.*, 2019, **25**, 2651–2662.
4 K. Singh, A. Kundu and D. Adhikari, *ACS Catal.*, 2022, **12**, 13075–13107.
5 Y. Umena, K. Kawakami, J. R. Shen and N. Kamiya, *Nature*, 2011, **473**, 55–60.
6 N. Ito, S. E. V. Phillips, C. Stevens, Z. B. Ogel, M. J. McPherson, J. N. Keen, K. D. S. Yadav and P. F. Knowles, *Nature*, 1991, **350**, 87–90.
7 J. Rittl and M. T. Green, *Science*, 2010, **330**, 933–937.
8 H. Schindelin, C. Kisker, J. Hilton, K. V. Rajagopalan and D. C. Rees, *Science*, 1996, **272**, 1615–1621.
9 P. J. Chirik and K. Wieghardt, *Science*, 2010, **327**, 794–795.
10 A. I. O. Suarez, V. Lyaskovskyy, J. N. H. Reek, J. I. van der Vlugt and B. de Bruin, *Angew. Chem., Int. Ed.*, 2013, **52**, 12510–12529.

11 D. L. J. Broere, B. de Bruin, J. N. H. Reek, M. Lutz, S. Dechert and J. I. van der Vlugt, *J. Am. Chem. Soc.*, 2014, **136**, 11574–11577.
12 D. L. J. Broere, N. P. van Leest, B. de Bruin, M. A. Siegler and J. I. van der Vlugt, *Inorg. Chem.*, 2016, **55**, 8603–8611.
13 D. Fujita, H. Sugimoto, Y. Shiota, Y. Morimoto, K. Yoshizawa and S. Itoh, *Chem. Commun.*, 2017, **53**, 4849–4852.
14 D. Fujita, H. Sugimoto, Y. Morimoto and S. Itoh, *Inorg. Chem.*, 2018, **57**, 9738–9747.
15 D. Fujita, A. Kaga, H. Sugimoto, Y. Morimoto and S. Itoh, *Bull. Chem. Soc. Jpn.*, 2019, **93**, 279–286.
16 Y. Ren, K. Cheaib, J. Jacquet, H. Vezin, L. Fensterbank, M. Orio, S. Blanchard and M. M. Desage-El, *Chem. – Eur. J.*, 2018, **24**, 5086–5890.
17 N. P. van Leest, M. A. Tepaske, J.-P. H. Oudsen, B. Venderbosch, N. R. Rietdijk, M. A. Siegler, M. Tromp, J. I. van der Vlugt and B. de Bruin, *J. Am. Chem. Soc.*, 2020, **142**, 552–553.
18 N. P. van Leest, M. A. Tepaske, B. Venderbosch, J.-P. H. Oudsen, M. Tromp, J. I. van der Vlugt and B. de Bruin, *ACS Catal.*, 2020, **10**, 7449–7463.
19 N. P. van Leest, J. I. van der Vlugt and B. de Bruin, *Chem. – Eur. J.*, 2021, **27**, 371–378.
20 N. P. van Leest and B. de Bruin, *Inorg. Chem.*, 2021, **60**, 8380–8387.
21 M. G. Chegerev, A. V. Piskunov, A. A. Starikova, S. P. Kubrin, G. K. Fukin, V. K. Cherkasov and G. A. Abakumov, *Eur. J. Inorg. Chem.*, 2018, **2018**, 1087–1092.
22 G. C. Briand, *Dalton Trans.*, 2023, **52**, 17666–17678.
23 H. Sugimoto, M. Yano, K. Sato, M. Miyanishi, K. Sugisaki, Y. Shiota, A. Kaga, K. Yoshizawa and S. Itoh, *Inorg. Chem.*, 2021, **60**, 18603–18607.
24 H. Braunschweig, B. Gehrhus, P. B. Hitchcock and M. F. Lappert, *Z. Anorg. Allg. Chem.*, 1995, **621**, 1922–1928.
25 F. E. Hahn, L. Wittenbecher, M. Kühn, T. Lügger and R. A. Fröhlich, *J. Organomet. Chem.*, 2001, **617–618**, 629–634.
26 F. E. Hahn, L. Wittenbecher, L. D. Van and A. V. Zabula, *Inorg. Chem.*, 2007, **46**, 7662–7667.
27 J. V. Dickschat, S. Urban, T. Pape, F. Glorius and F. E. Hahn, *Dalton Trans.*, 2010, **39**, 11519–11521.
28 M. M. Huang, M. M. Kireenko, E. K. Lermontova, A. V. Churakov, Y. F. Oprunenko, K. V. Zaitsev, D. Sorokin, K. Harms, J. Sundermeyer, G. S. Zaitseva and S. S. Karlov, *Z. Anorg. Allg. Chem.*, 2013, **639**, 502–511.
29 S. Krupski, R. Pöttgen, I. Schellenberg and F. E. Hahn, *Dalton Trans.*, 2014, **43**, 173–181.
30 J. Brugos, J. A. Cabeza, P. García-Álvarez, E. Pérez-Carreño and D. Polo, *Dalton Trans.*, 2018, **47**, 4534–4544.
31 Y. Mizuhata, T. Sasamori and N. Tokitoh, *Chem. Rev.*, 2009, **109**, 3479–3511.
32 K. Goto, G. Yamamoto, B. Tan and R. Okazaki, *Tetrahedron Lett.*, 2001, **42**, 4875–4877.
33 S. Paria, T. Ohta, Y. Morimoto, T. Ogura, H. Sugimoto, N. Fujieda, K. Goto, K. Asano, T. Suzuki and S. Itoh, *J. Am. Chem. Soc.*, 2015, **137**, 10870–10873.
34 D. V. Yandulov and R. R. Schrock, *Science*, 2003, **301**, 76–78.
35 R. Hani and R. A. Geanangel, *Coord. Chem. Rev.*, 1982, **44**, 229–246.
36 T. Heidemann and S. Mathur, *Eur. J. Inorg. Chem.*, 2014, **2014**, 506–510.
37 Z. Qianqian, X. Bo, D. Mengzhen, L. Gongqiang, T. Ailing and Z. Erjun, *J. Mater. Chem. C*, 2018, **6**, 10902–10909.
38 A. K. Dhiman, S. Gupta, R. Sharma, R. Kumar and U. Sharma, *J. Org. Chem.*, 2019, **84**, 12871–12880.
39 S.-H. Hwang, H. Kim, H. Ryu, I. E. Serdiuk, D. Lee and T.-L. Choi, *J. Am. Chem. Soc.*, 2022, **144**, 1778–1785.
40 J. V. Ruppel, R. M. Kamble and X. P. Zhang, *Org. Lett.*, 2007, **9**, 4889–4892.
41 F. Sebest, L. Casarrubios, H. S. Rzepa, A. J. P. White and S. Díez-González, *Green Chem.*, 2018, **20**, 4023–4035.
42 S. Stol and A. Schweiger, *J. Magn. Reson.*, 2006, **178**, 42–55.
43 G. Sheldrick, *Acta Crystallogr., Sect. A: Found. Adv.*, 2015, **71**, 3–8.
44 O. V. Dolomanov, L. J. Bourhis, R. J. Gildea, J. A. K. Howard and H. Puschmann, *J. Appl. Crystallogr.*, 2009, **42**, 339–341.
45 M. J. Frisch, G. W. Trucks, H. B. Schlegel, G. E. Scuseria, M. A. Robb, J. R. Cheeseman, G. Scalmani, V. Barone, G. A. Petersson, H. Nakatsuji, X. Li, M. Caricato, A. V. Marenich, J. Bloino, B. G. Janesko, R. Gomperts, B. Mennucci, H. P. Hratchian, J. V. Ortiz, A. F. Izmaylov, J. L. Sonnenberg, D. Williams-Young, F. Ding, F. Lipparini, F. Egidi, J. Goings, B. Peng, A. Petrone, T. Henderson, D. Ranasinghe, V. G. Zakrzewski, J. Gao, N. Rega, G. Zheng, W. Liang, M. Hada, M. Ehara, K. Toyota, R. Fukuda, J. Hasegawa, M. Ishida, T. Nakajima, Y. Honda, O. Kitao, H. Nakai, T. Vreven, K. Throssell, J. A. Montgomery Jr., J. E. Peralta, F. Ogliaro, M. J. Bearpark, J. J. Heyd, E. N. Brothers, K. N. Kudin, V. N. Staroverov, T. A. Keith, R. Kobayashi, J. Normand, K. Raghavachari, A. P. Rendell, J. C. Burant, S. S. Iyengar, J. Tomasi, M. Cossi, J. M. Millam, M. Klene, C. Adamo, R. Cammi, J. W. Ochterski, R. L. Martin, K. Morokuma, O. Farkas, J. B. Foresman and D. J. Fox, *Gaussian 16, Revision A. 03*, Gaussian, Inc., Wallingford, CT, 2016.
46 A. D. Becke, *J. Chem. Phys.*, 1993, **98**, 5648–5652.
47 C. Lee, W. Yang and R. G. Parr, *Phys. Rev. B: Condens. Matter Mater. Phys.*, 1988, **37**, 785–789.
48 G. Igel-Mann, H. Stoll and H. Preuss, *Mol. Phys.*, 1988, **65**, 1321–1328.
49 A. Bergner, M. Dolg, W. Kuechle, H. Stoll and H. Preuss, *Mol. Phys.*, 1993, **80**, 1431–1441.
50 T. H. Dunning Jr. and P. J. Hay, in *Modern Theoretical Chemistry*, ed. H. F. Schaefer III, Plenum, New York, 1977, vol. 3, pp. 1–28.